Proceedings of ASME Turbo Expo 2011
GT2011
June 6-10, 2011, Vancouver, British Columbia, Canada

GT2011-46051

NUMERICAL RESEARCH OF THE RAM-ROTOR WITH DIFFERENT GEOMETRIC PARAMETERS

Ling Yang
Marine Engineering College
Dalian Maritime University
Dalian 116026 China
7331yangling@163.com

Jingjun Zhong
Marine Engineering College
Dalian Maritime University
Dalian 116026 China

Ji-ang Han
Marine Engineering College
Dalian Maritime University
Dalian 116026 China

ABSTRACT

With the design methods of typical supersonic aircraft intakes and the advantages of shock wave compression, ram-rotors have become a new attractive compression system. Lots of research work has been carried out on rampressors, but the influence of the geometric parameters on the shock wave structure and compression performance of the ram-rotor has not been studied systematically. Therefore, a thorough study on ram-rotor with different geometric parameters is required.

In this paper, a steady three-dimensional Navier-Stokes equation adopted in the “Fluent” software package is carried out on a large parallel computer. Six factors which may influence the ram-rotor performance are investigated numerically. These geometric parameters are strake section shape, throat length-height ratio, strake stagger angle, compression ramp angle, subsonic divergent angle and throat contraction ratio. The study is composed of two parts. The aim of the first part is to understand the influence of the geometric parameters listed above on the shock wave structure and compression performance of the ram-rotor by comparison and analysis of the relative Mach number and static pressure in the flow-path. The aim of the second part is to obtain the optimal geometric structure of the ram-rotor by comparison and analysis of the structure of the flow fields, the compression performance and the ram-rotor properties.

First of all, the numerical method is validated by comparing the numerical results of the flow field of a supersonic intake with experimental results in this paper. Secondly, the flow field structures in the ram-rotor, especially the number and position of shock waves and the separation zone, are studied. Thirdly, the influence of the geometric parameters on the rotor performance is studied. Some parameter distributions, such as the flow angle, adiabatic efficiency, total pressure ratio, total pressure recovery coefficient, are compared and analyzed. The rules of the ram-rotor performance variation with different geometric parameters are also presented. Finally, some advice for improving the overall performance of the ram-rotor is given according to the flow field analysis.

NOMENCLATURE

R_y	Radius of the points on the compression ramp
R_l	Rim radius of the ram-rotor
R_t	Radius of the points on the throat
R_k	Radius of the points on the hub in subsonic diffuser
$\Delta\theta_1$	Central angle difference between two points on the compression ramp
$\Delta\theta_2$	Central angle difference between two points on the hub in subsonic diffuser
θ_t	Central angle corresponding to the length of throat
$\Delta\theta_t$	Central angle difference between two points on the throat
l_t	Throat length
h_t	Throat height
h_i	Strake height at inlet
α	Strake section shape angle (Fig. 10)
δ	Compression ramp angle
γ	Subsonic divergent angle
ϕ	Strake stagger angle
z_y	z coordinate of the points on the compression ramp
z_t	z coordinate of the points on the throat
z_k	z coordinate of the points on the hub in subsonic diffuser
p_1^*	Absolute total pressure at inlet
p_2^*	Absolute total pressure at exit
p_1	Static pressure at inlet
p_2	Static pressure at exit

p_{1rel}^* Relative total pressure at inlet
p_{2rel}^* Relative total pressure at exit
T_1^* Absolute total temperature at inlet
T_2^* Absolute total temperature at exit
k Adiabatic exponent
π^* Total pressure ratio
π static pressure ratio
σ Total pressure recovery coefficient
η^* Adiabatic efficiency

1 INTRODUCTION

Shock wave compression technology[1] is a method that uses shock waves made by supersonic flow passing an object to compress flow and is often applied to supersonic aircraft intakes[2~4]. Compared to the traditional axial-flow and centrifugal-flow compression methods, the shock wave compression has high pressure ratio, potential high efficiency, simple structure, light weight and less rotating parts. So the shock wave compression method has a huge potential application merit. However, it must satisfy the supersonic inlet condition. If the method can be used under low speed inlet conditions, the range of its application will be enlarged enormously and a new direction to advance and improve compressor performance will also be established. In order to use shock wave compression for subsonic inlet conditions, we can make a rotor with high circumferential speed, so the relative speed on the rim of the rotor can reach or exceed the local velocity of the sound. Based on this thinking, a new kind of compression system is designed, called the Ramprssor compressor[5] which has high performance [6~8]. If we use Rampressor compressor to substitute the traditional compressor in aeroengine, the thrust-weight ratio of the aeroengine would be significantly increased [9].

A lot of research work has been carried out in great depth on the Rampressor[10~13]. However, how the geometric parameters influence on the shock wave structure and compression performance of ram-rotor [5, 14], has not been publicly reported. So a systematical study on the ram-rotor with different geometric parameters is required. In this paper, six factors that may influence the ram-rotor performance are studied. These geometric parameters are strake section shape, throat length-height ratio, strake stagger angle, compression ramp angle, subsonic divergent angle and throat contraction ratio.

2 DESIGN OF THREE DIMENSIONAL FLOW-PATH

The structure of the three dimensional flow-path of the ram-rotor will affect the compression performance and efficiency of the ram-rotor. This can be investigated as the bending deformation of a supersonic intake (Fig. 2[6]). Therefore the three dimensional flow-path of the ram-rotor is designed referring to the design methods of a three dimensional supersonic intake.

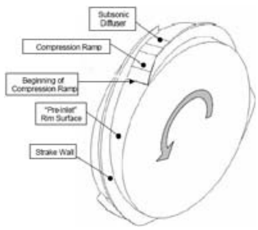

Fig.1 New supersonic compressor concept "Ramgen" [5]

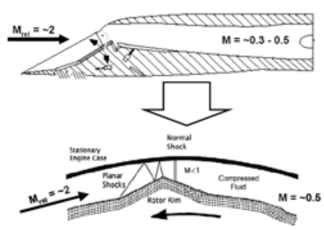

Fig.2 Flight inlet schematic (upper), Shock structure in conceptual rotor (lower) [6]

The radius of the points on the compression ramp can be calculated by using the following formula

$$R_y = R_l \cdot e^{\Delta\theta_1 \cdot \tan\delta}$$

The central angle corresponding to the length of the throat is

$$\theta_t = \frac{l_t}{R_t}$$

The radius of the points on the hub in the subsonic diffuser can be given as

$$R_k = R_t \cdot e^{\Delta\theta_2 \cdot \tan\gamma}$$

The z coordinate of the points on the compression ramp, the throat and the hub are

$$z_y = R_l \cdot \tan\phi \cdot \Delta\theta_1$$
$$z_t = R_l \cdot \tan\phi \cdot (\Delta\theta_1 + \Delta\theta_t)$$
$$z_k = R_l \cdot \tan\phi \cdot (\Delta\theta_1 + \Delta\theta_t + \Delta\theta_2)$$

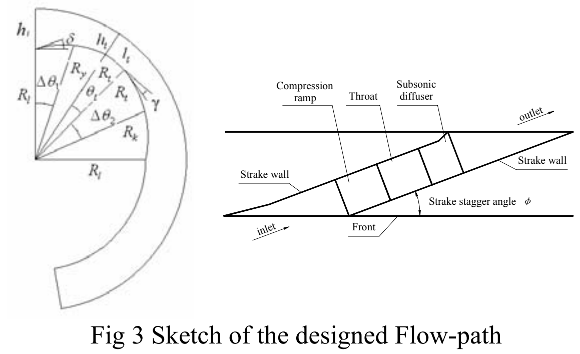

Fig 3 Sketch of the designed Flow-path

Based on the expression above, the sketch of the designed Flow-path is shown in Fig. 3, the generatrix of the compression ramp, the throat and the hub is then obtained.

The leading edges of the strake are sharpened (Fig. 4) in order to reduce the inlet resistance and the ram-rotor weight. The trailing edges are also

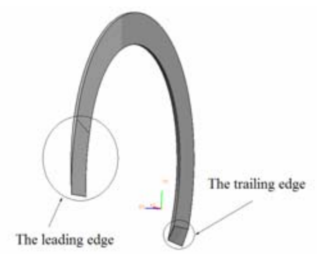

Fig.4 The leading and trailing edges of ram-rotor strake

treated with the same method (Fig. 4) to reduce the weight of the ram-rotor furtherly and use the lateral extension of the strake to compress the air flow.

3 MUMERICAL MODEL AND METHOD

3.1 GRIDS AND BOUNDARY CONDITIONS

The block-structured grids (Fig. 5) are adopted to the computational domain, and for saving the computing resources and fasting the computing speed, only one flow-path is numerically simulation in this paper. Because the structures are different with different geometric parameters, the total grid number is not complete same as each other, which will be shown in different part of this paper.

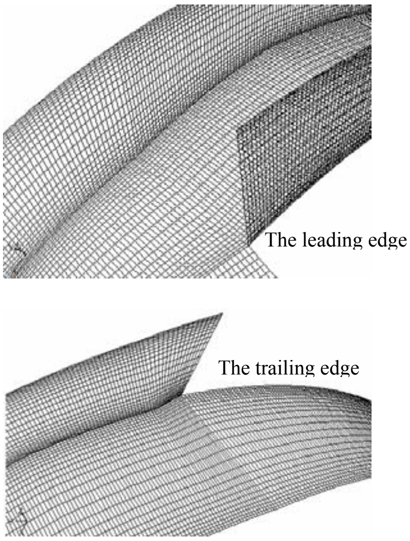

Fig 5 Computational grids

The boundary conditions used in the numerical simulation include inlet boundary condition, outlet boundary condition, periodic boundary condition and wall boundary condition (Fig. 6). At the inlet of the flow-path, the total pressure, static pressure, total temperature and the direction of incoming flow should be given. The hub and the side walls of the flow-path are set as adiabatic walls which have the same rotational speed with the working fluid, and the casing is set as adiabatic wall which is absolutely stationary, and all solid surfaces are no-slip in the relative frame. The side walls of the inlet part and the outlet part are set as periodic boundary.

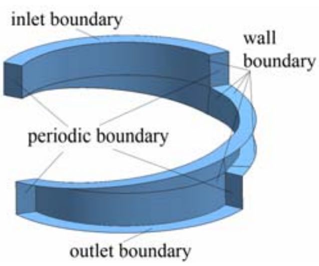

Fig 6 Computational domain and boundary conditions

3.2 NUMERICAL METHOD

As one kind of popular computational fluid dynamics software [15] [16], "Fluent" software package is adopted to simulate numerically the flow field of the designed flow-path in this paper. A three-dimensional steady Reynolds averaged Navier-Stokes equations composed in "Fluent" Software Pack is carried out in a large parallel computer. The turbulent model used in this paper is the S-A model, a relatively simple one-equation model that solves a modeled transport equation for the involving wall-bounded flows, which has been shown to give good results for boundary layers subjected to adverse pressure gradients. The coupled implicit solution method is used to solve the control equations, and the second order upwind scheme is used to discrete the convection term in the control equations.

4 VALIDATION OF NMMERICAL METHOD

The numerical method is validated by comparing the numerical results of the flow field of a supersonic intake with its experimental results. The initial conditions, the boundary conditions, the geometric parameters of the intake and the experimental results are taken as same as that in reference [17]. The wall pressure distribution, the flow separation, and the critical shock wave/boundary layer interaction in the numerical simulation show a good agreement with the experimental results (Fig. 7~9). Because it gives good results for the resolution of the shock wave system and flow separation, the numerical method adopted in this paper is feasible to solve supersonic compressible flow.

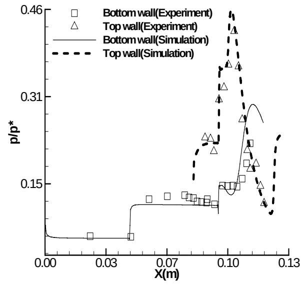

Fig. 7 Comparison of wall pressure distribution[17]

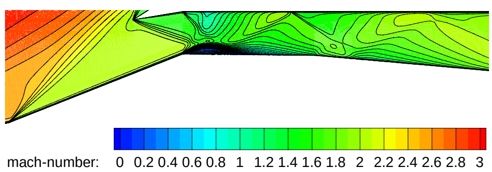

Fig. 8 Local Mach number contour of numerical simulation

Fig. 9 Local Mach number contour of experimental result[17]

In this paper, the geometric parameters are different between the supersonic intake and the ram-rotor, so the grid density and sensitivity should be considered separately. Taking case A1 as an example (Table 1), the grid number of the radial, the flow direction and pitch direction are all refined, and the total grid number is about 515000, 770000 and 950000, respectively. The grid density has some influence on the flow field (Fig. 11), but the distribution of the shock waves and the separation zones are basically identical. When the total grid number is 770000, the last reflected shock wave is clearer than that of 515000. The grid density also leads the change of the total pressure at exit (Fig. 10(d)), and the difference of total pressure ratio in these three cases is less than 0.3. For the high total pressure ratio (more than7), this difference can be accepted.

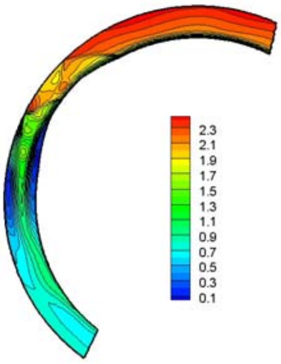

(a) grid 515000

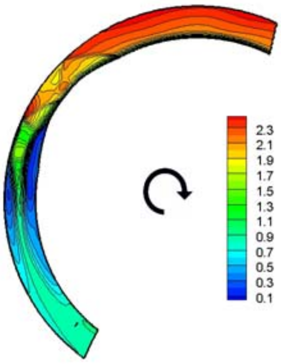

(b) grid 770000

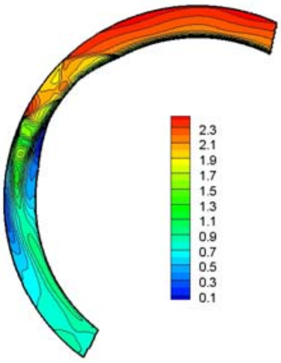

(c) grid 950000

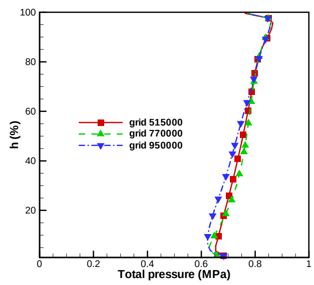

(d) Total pressure

Fig.10 Relative Mach number contour of S2 flow surface at 50% pitch of the flow-path and distribution of total pressure at exit

The total grid number keeps invariant, and the local grid is refined, namely, the radial ratio varies from 1.2 to 1.36 and the pitch direction varies from 1.15 to 1.3. Because high density grid near the wall leads the middle flow-path grid number reduces, the last reflected shock wave is most vague among these three cases (Fig. 11(a)-(c)). The trends of total pressure at exit are similar each other (Fig. 11(d)), and the difference of total pressure ratio in these three cases is less than 0.06. So, the grid refinement setting as case A1 can be accepted, and the average wall y+ of case A1 values about 250.

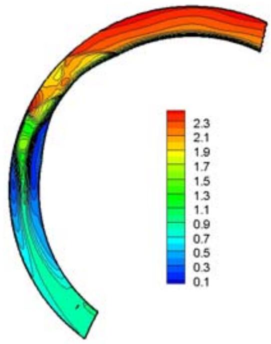

(a) grid 770000-1

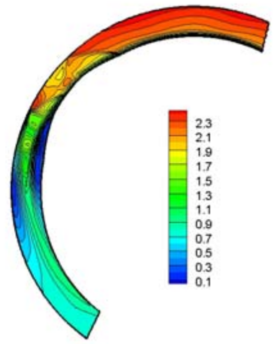

(b) grid 770000-2

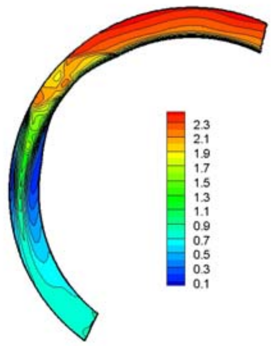

(c) grid 770000-3

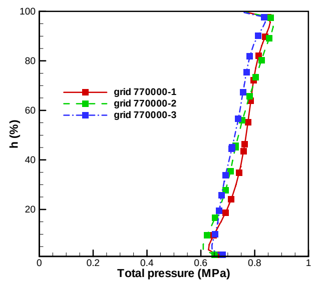

(d) Total pressure

Fig.11 Relative Mach number contour of S2 flow surface at 50% pitch of the flow-path and distribution of total pressure at exit

In order to facilitate the analysis, the concept of S1 and S2 flow surface in turbomachinery is used to analyze the computational results of the ram-rotor three dimensional flow-path. The width of the flow-path is defined as pitch (t), and the direction along the width of the flow-path is defined as pitch wise, as shown in Fig. 12.

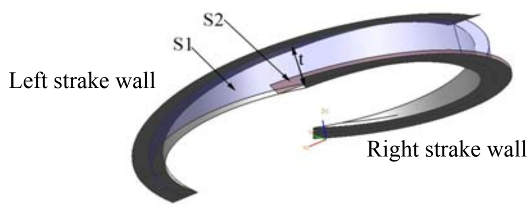

Fig. 12 Definition of flow field representative method

Performance parameters can be calculated by using the following formulas

$$\pi^* = \frac{p_2^*}{p_1^*} \qquad (1)$$

$$\pi = \frac{p_2}{p_1} \qquad (2)$$

$$\sigma = \frac{p_{2rel}^{*}}{p_{1rel}^{*}} \qquad (3)$$

$$\eta^{*} = \frac{\pi^{*\frac{k-1}{k}} - 1}{\frac{T_2^{*}}{T_1^{*}} - 1} \qquad (4)$$

Six geometric parameters which may influence the ram-rotor flow field and performance, the strake section shape, throat length-height ratio, strake stagger angle, compression ramp angle, subsonic divergent angle and throat contraction ratio, are studied respectively. For comparison and analysis with different geometric parameters of the ram-rotor's flow field and performance, all cases are defined as Table 1.

Table 1 Geometric parameters of the Ram-rotor

Case	Strake section shape (α)	Throat length-height ratio (h_l/h_t)	Strake stagger angle (ϕ)	Compression ramp angle (δ)	Subsonic divergent angle (γ)	Throat contraction Ratio (h_t/h_i)
A1	α_2=4°					
A2	α_2=6°	2	8°	8°	7°	0.8
A3	α_2=8°					
B1		1				
B2	α_2=4°	3	8°	8°	7°	0.8
B3		4				
C1			10°			
C2			12°			
C3	α_2=4°	2	14°	8°	7°	0.8
C4			16°			
C5			18°			
D1				6°		
D2	α_2=4°	2	8°	7°	7°	0.8
D3				9°		
E1					6°	
E2	α_2=4°	2	8°	8°	8°	0.8
E3					9°	
F1						0.6
F2	α_2=4°	2	8°	8°	7°	0.7
F3						0.9

5 RESULTS AND DISCUSS

5.1 STRAKE SECTION SHAPE

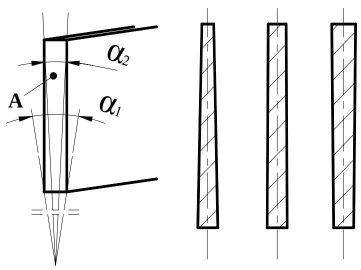

(a) (b) (c) (d)

Fig. 13 Sketch of strake wall section shape

The three dimensional flow-path with three kinds of strake section shape is numerical studied at the design point. As shown in Fig. 13, the plane A perpendiculars to the axis, including α_1 and α_2, respectively. The strake section shape of Fig.13 (b) and (c) is positive trapezoid; in contrary, the shape of Fig. 13 (d) is reversed trapezoid. α_1 in all cases is 8°, α_2 in case A1, A2 and A3 is 4°, 6°and 8°, respectively. For studying the strake section shape, other geometric parameters keep invariant (Table 1). The total grid number is about 7.7×10^5. The initial conditions of the numerical simulation in cases A1~A3 are listed in Table 2.

Table 2 Initial conditions of the numerical simulation in cases A1~A3

Ma_0	P (Pa)	T_0 (K)	N (rpm)
0.30618	94947	288.15	34223

It is found that there are several curve shock waves in the three dimensional flow-path, and all shock wave strains stay steadily attached to the throat exit(Fig. 14). Both near the casing and the hub in case A1 have one separation zone. The start position of the hub separation zone is near the throat exit and the separation zone extends to the flow-path exit. The hub separation zone in the cases A2 and A3 is vague, but the casing separation zone is bigger than that of case A1. Under the same boundary conditions, the point of intersection between the second reflected shock wave and the casing separation zone of the cases A1, A2 and A3 move towards to the inlet in turn, and the mass flow decrease from 4.53 kg/s to 4.45 kg/s and 4.38 kg/s, respectively. Though the hub width of strake wall section shapes are same among the three cases, the casing width increases with α_2, so the airflow passage area near the casing is smaller than that of near the hub, which induces the change of the separation zone, the reflect point and the mass flow.

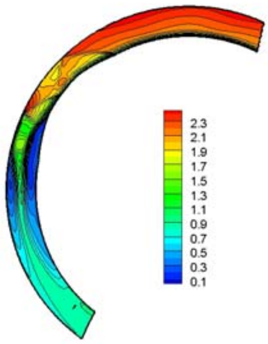

(a) case A1

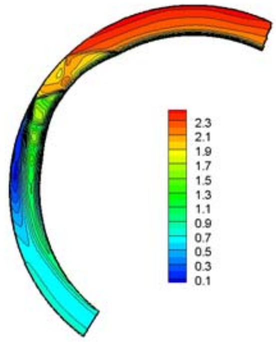

(b) case A2

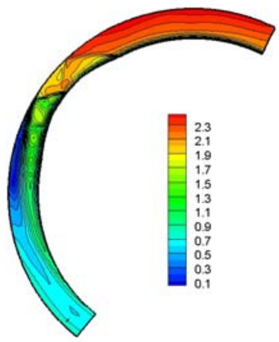

(c) case A3

Fig. 14 Relative Mach number contour of S2 flow surface at 50% pitch of the flow-path

The flow field changes with the increase of α_2, but the trend is similar with each other. The top curves in Fig. 15(a) and the bottom curves in Fig. 15(b) are corresponding to the right strake wall, and the bottom curves in Fig. 15(a) and the top curves in Fig. 15(b) are corresponding to the left strake wall, respectively. The abscissa is the relative axial length and the ordinate is the static pressure and the relative Mach number.

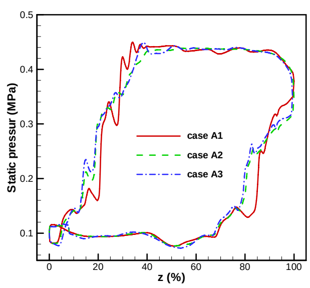

(a)

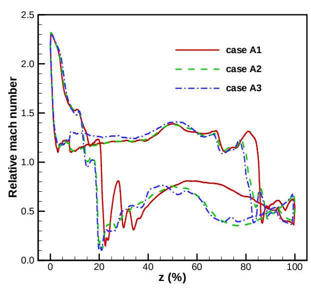

(b)

Fig 15 Static pressure and relative Mach Number of strake wall

There are static pressure increase and relative Mach number decrease in the forepart axial length of the right strake wall (Fig. 15), and the change position is between the compress ramp start position and the throat exit.

On the right strake wall, the first intersection of the reflected shock wave and the hub is near the throat inlet, so there is one large pressure increase there. And the flow-path is divergent at the throat outlet, so another large pressure increase occurs. After a series of different degree waves, the static pressure is stable, and the flow velocity is subsonic.

On the left strake wall, the static pressure and relative Mach number are stable before about 70% relative axial length and the different for three cases is not obvious. But after that length, there is a certain degree of static pressure increases and relative Mach number decreases because the positions are located after the throat exit. In this divergent zone, the relative Mach number changes from supersonic to subsonic. Under the same boundary conditions, the positions of pressure increase and Mach number decrease move towards the inlet, because the wall affects the shock waves and the air flow at a certain degree, and the increase of strake wall section leads to the decrease of the flow-path section.

The total pressure and the total temperature increase gradually along the radial because the inlet relative Mach number increases gradually along the radial direction (Fig. 16). Comparing to other two cases, the flow parameters distribution in case A1 are relative uniform.

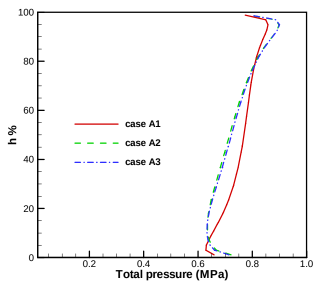

(a)

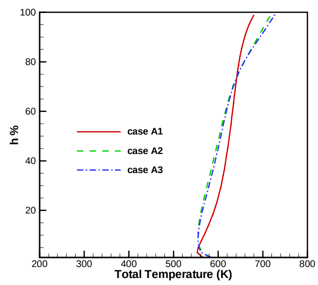

(b)

Fig 16 Distribution of flow parameters at exit

Flow angle which is the angle between the airflow direction and the axis in these three cases (Table 3) is larger than that of traditional axial or centrifugal compressor because the strake stagger angle is only 8°. Comparing to the other two cases, case A1 has the smallest flow angle. Because there are many shock waves in the three dimensional flow-path and the shock wave loss is inevitable. In addition, the strong flow separation in the subsonic diffuser also results in the increasing of flow loss, all adiabatic efficiencies are lower in these three cases, only 71 to 73 percent. But with increase of α_2, the flow-path section decreases and airflow separates seriously and adiabatic efficiency reduces.

Table 3 Performance parameters of ram-rotor at exit with different α_2

α_2	4°	6°	8°
Flow angle (°)	82.36	83.48	83.41
Adiabatic efficiency	0.7229	0.7163	0.7135

5.2 THROAT LENGTH –HEIGHT RATIO

At design point, the three dimensional flow-path of the ram-rotor with four kinds of throat length-height ratio is numerically simulation. The throat length-height ratios in cases B1, A1, B2 and B3 are 1, 2, 3 and 4, respectively, and other geometric parameters keep invariant (Table 1). Because the throat length-height ratio is different, the total grid number changes from about 7.7×10^5 to 8.1×10^5. The initial conditions of numerical simulation are listed in Table 2. The shock wave stains and the starting position of the separation zone are stably located at the exit of the throat by adjusting the back pressure in computing process.

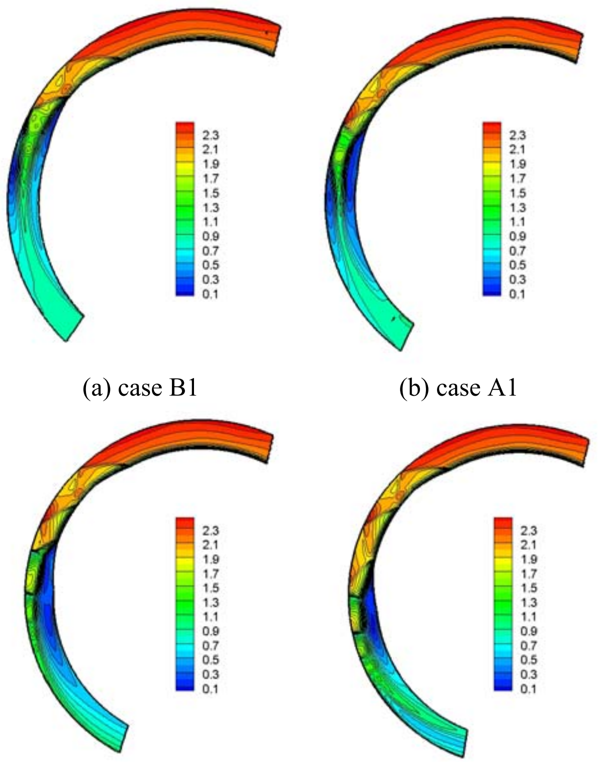

(a) case B1 (b) case A1

(c) case B2 (d) case B3

Fig.17 Relative Mach number contour of S2 flow surface at 50% pitch of the flow-path

The shock waves and the flow field structure are obviously affected by the throat length-height ratio (Fig. 17). There are three shock waves in the three dimensional flow-path, including one incident wave and two reflected shock waves. The separation zone near the casing is slightly larger than that near the hub. There are four curve shock waves in case A1 and the area of the two separation zone at the casing and hub are similar to each other. There are five curve shock waves in case B2, which the throat length-height ratio is 2. The most difference between case B2 and case A1 is that case B2 has only one separation zone attached to the hub in the flow-path. With the flow moves downwards, the separation zone occupies the whole flow-path. With the throat length increases, there are six curve shock waves in the flow-path of case B3.

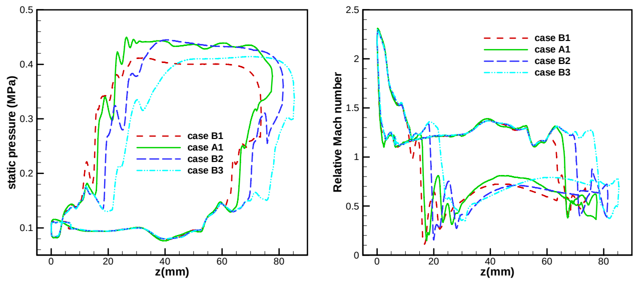

（a） （b）

Fig. 18 Static pressure and relative Mach number of strake wall at 50 % throat height

There also have several pressure increase and relative Mach number decrease (Fig. 18). With the reduction of the throat length-height ratio, the positions of these pressure increase and Mach number decrease move towards the flow-path inlet.

With the increase of throat length-height ratio, the flow angle rises. Under the same boundary conditions, the smaller the flow angle is expected. Among these four cases, the flow angle of case B1 is the smallest, but the adiabatic efficiency and the total pressure ratio are the lowest, too. Case A1 has the highest adiabatic efficiency and the highest total pressure ratio among these cases, though the flow angle of case A1 is slightly larger than case B1. With the increase of the throat length-height ratio, the flow angle increases. Both case B1 and B2 have lower adiabatic efficiency and total pressure ratio than those of case A1. In addition, the bigger the throat length-height ratio, the wider the ram-rotor, for example, case B2 is wider 5% than that of case A1. So, case A1 has the optimal throat length-height ratio, compromised among the flow angle, the adiabatic efficiency, the total pressure, the ram-rotor width, etc.

Table 4 Performance parameters of the ram-rotor at exit with different throat length-height ratio

Throat length-Height ratio	1	2	3	4
Flow angle (°)	81.91	82.36	84.35	84. 87
Adiabatic efficiency	0.6980	0.7229	0.7156	0.7163
Total pressure ratio	6.2383	7.0970	6.9662	6.6132

5.3 STRAKE STAGGER ANGLE

Stagger angle is defined as the angle between the strake and the front (Fig. 3), the strake stagger angle in case A1, C1, C2, C3, C4 and C5 are 8°, 10°, 12°, 14°, 16°and 18°, respectively. In order to compare and analysis the influence of strake stagger angle on the flow field and performance of the ram-rotor, other geometric parameters keep invariant (Table 1). Because the strake stagger angles are different in the cases listed above, the total grid number changes from about 7.7×10^5 to 11.1×10^5. Under the same inlet relative Mach number condition, the rotational speed and inlet pressure are different. So the shock wave stains and the starting positions of separation zones are stably located at the exit of the throat by adjusting the back pressure in computing process.

It is found that the strake stagger angle has almost no effect on the shock waves number and distribution (Fig. 19). There are four main curve shock waves in the flow-path. The flow field structure changes with the increase of the strake angle, case A1 has two separation zones attached to the casing and the hub, but each case has only one separation zone near the hub after the strake stagger angle 10°, the separation zone is dominant in the subsonic diffuser and the difference among these relative Mach number contour of S2 flow surfaces at 50% pitch of the flow-path is not obvious.

Some performance parameters of the ram-rotor are listed in Table 5. Under the same inlet relative Mach number condition, with the increase of the strake stagger angle, the inlet axial speed and the mass flow rate rise, the mass flow rate with the strake stagger angle 18° is about double that of 8°. At the same time, the rotational speed decreases which would benefit to select the material of the ram-rotor and the shaft. With the increase of the strake stagger angle, the flow angle reduces rapidly because the axial speed rises and the rotational speed decreases. The higher the strake stagger angle, the lower the total pressure ratio, adiabatic efficiency and total pressure recovery coefficient. The width ratio is defined as the ratio between the width in different case with the width in case A1. Case A1 has the highest total pressure ratio and the thinnest width of the ram-rotor, but the flow angle and mass flow rate are slightly smaller. Case C2 has the highest adiabatic efficiency and total pressure recovery coefficient, but the total pressure ratio declines 0.8, and the width of the ram-rotor is 50% wider. Case C5 has the smallest flow angle and the largest flow mass, but the adiabatic efficiency and the total pressure ratio are lowest, even the width is more than double that of case A1. Therefore, the reasonable compromise is needed among these performances. For example, if the total pressure ratio is the emphasis, the highest adiabatic efficiency and the flow angle have to be compromised.

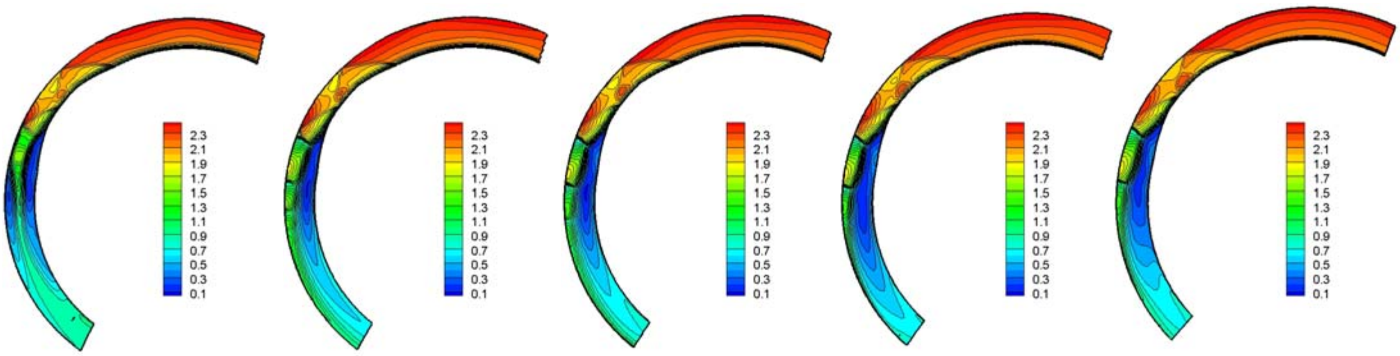

(a) case A1 (b) case C1 (c) case C2 (d) case C3 (e) case C5

Fig.19 Relative Mach number contour of S2 flow surface at 50% pitch of the flow-path

Table 5 Performance parameters of the ram-rotor at exit with different strake stagger angles

Strake stagger angle	8°	10°	12°	14°	16°	18°
Flow angle (°)	82.36	81.97	78.92	77.80	76.27	74.94
Adiabatic efficiency	0.7229	0.7226	0.7336	0.7284	0.7202	0.7097
Total pressure recovery coefficient	0.5731	0.6015	0.6552	0.6278	0.6027	0.5843
Total pressure ratio	7.0970	6.8067	6.2771	6.2578	6.0499	5.8078
Mass flow rate (kg/s)	4.5294	5.6008	6.6609	7.6226	8.4861	9.2603
Width ratio	1.00	1.25	1.49	1.73	1.96	2.19

5.4 COMPRESSION RAMP ANGLE

Three dimensional flow field in the flow-path of the ram-rotor with four kinds of compression ramp angle are studied. The compression ramp angle in case D1, D1, A1 and D3 are 6°, 7°, 8°and 9°, respectively. Each case's total grid number is about 7.7×10^5. The back pressure is adjusted in computing process to stabilize the shock wave stain. The starting position of separation zone locates at the throat exit.

There are three curve shock waves and one separation zone (Fig. 20(a)-(b)). With the increase of compression ramp angle, the shock wave number adds up to 4, and the separation zone has the trend of moving towards the hub. Case A1 has two separation zones, and case D3 has only one separation zone attached to the hub, which almost occupies the whole flow-path. This demonstrates that the compression ramp angle has a certain degree effect on the shock wave and field structure of the ram-rotor.

Compare to the cases with different strake stagger angles, the performance parameters change only a small range with different compression ramp angles (Table 6). With the increase of the compression ramp angle, the flow angle and the total pressure recovery coefficient reduce slightly, and the total pressure ratio rises firstly and then decreases, the fluctuation range is narrow. Case A1 has the highest adiabatic efficiency among all the cases, but the trend is irregular.

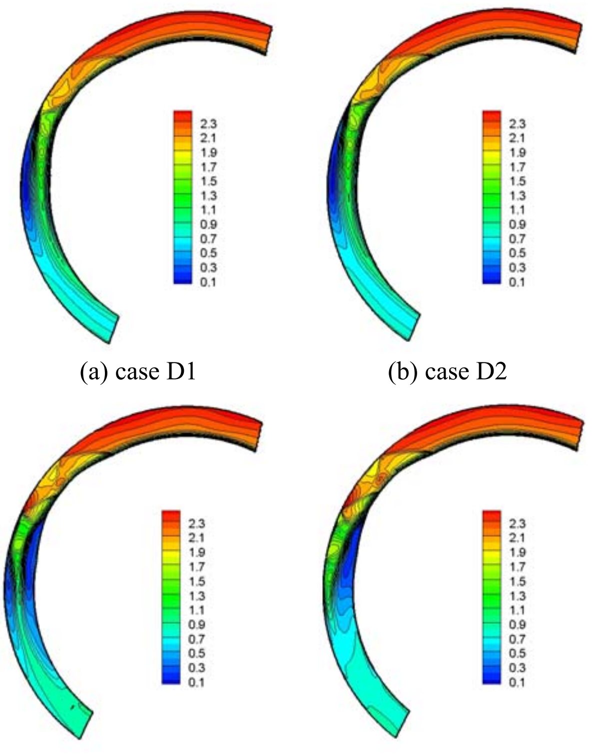

(a) case D1 (b) case D2

(c) case A1 (d) case D3

Fig.20 Relative Mach number contour of S2 flow surface at 50% pitch of the flow-path

Table 6 Performance parameters of ram-rotor at exit with different compression ramp angles

Compression ramp angle	6°	7°	8°	9°
Flow angle (°)	83.58	83.52	82.36	82.81
Adiabatic efficiency	0.7214	0.7188	0.7229	0.7110
Total pressure recovery coefficient	0.6145	0.5935	0.5731	0.5496
Total pressure ratio	7.1092	7.1131	7.0970	6.9025

5.5 SUBSONIC DOVERGENT ANGLE

The subsonic divergent angle in case E1, A1, E2 and E3 are 6°, 7°, 8°and 9°, respectively. Each case's total grid number is also about 7.7×10^5. Computing process is the same as that of compression ramp angles.

Similar to the compression ramp angle, the separation zone in the flow-path has the trend of moving towards the hub with the increase of the subsonic divergent angle (Fig. 21). When subsonic divergent angle is less than 8°, there are two separation zones attached to both the casing and the hub. When it is more than 8°, the casing separation zone almost disappears, and separation zone only exists attached to the hub. Furthermore, it seems that subsonic divergent angle has not too much effect on the number and distribution of shock waves.

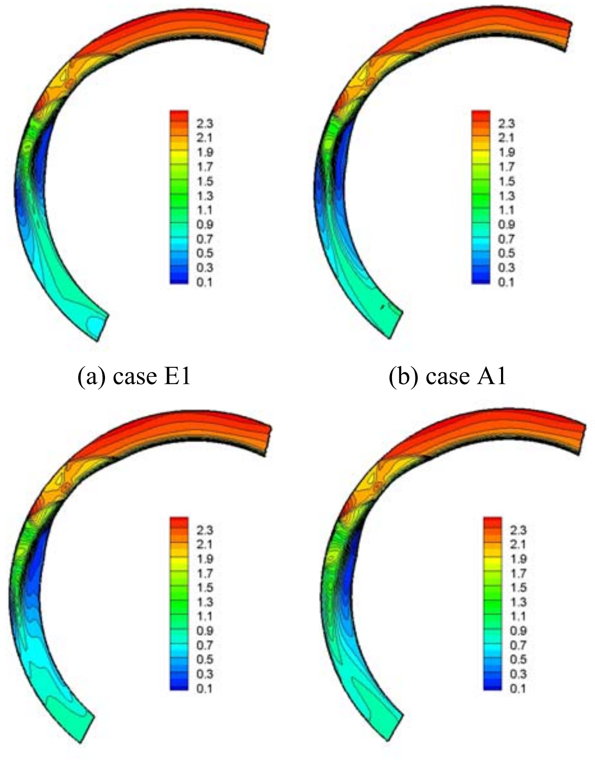

(a) case E1 (b) case A1

(c) case E2 (d) case E3

Fig.21 Relative Mach number contour of S2 flow surface at 50% pitch of the flow-path

With the increase of subsonic divergent angle, the flow angle and total pressure ratio decreases at the first and then climbs up in a certain degree (Table 7). The trends of the adiabatic efficiency and total pressure recovery coefficient are reverse compared to the trends of the flow angle and total pressure ratio.

Table 7 Performance parameters of ram-rotor at exit with different subsonic divergent angles

Subsonic divergent angle	6°	7°	8°	9°
Flow angle (°)	82.83	82.36	83.06	84.14
Adiabatic efficiency	0.7165	0.7229	0.7184	0.7169
Total pressure recovery coefficient	0.5574	0.5731	0.5693	0.5632
Total pressure ratio	7.4623	7.0970	6.7276	6.7716

5.6 THROAT CONTRACION RATIO

The throat contraction ratio is defined as the ratio between the throat height with the inlet height. The throat contraction ratios of case F1, F2, A1 and F3 are 0.6, 0.7, 0.8 and 0.9, respectively. Each case's total grid number is still about 7.7×10^5. Computing process is the same as that of compression ramp angles.

The throat contract ratio has an important influence on the shock wave and the flow field structure (Fig. 22). With the increase of the throat contraction ratio, the shock wave number reduce from seven to three. The reason is that for the same geometric parameters, the smaller the throat contraction ratio, the longer the compression ramp and the more the reflected shock waves. The position of the separation zone moves from the hub towards the casing. There is one separation zone in case F1 and case F2 attached to the hub. There are two separation zones in case A1, only one in case F3 attached to the casing.

The change of the throat contraction ratio results in a wide range change of all performance parameters (Table 8). With the decrease of throat contract ratio, the total pressure ratio, adiabatic efficiency and total pressure recovery coefficient increase. Case F1 has the highest total pressure ratio, more than 12.2, and adiabatic efficiency is also higher than those cases with bigger throat contraction ratio (case A1 and case F3). It is found that if the throat contraction ratio changes from 0.7 to 0.6, the total pressure ratio increases from 8.9 to 12.2, it's a big change because the compression ramp is longer in case F1 causing a larger amount of reflected shock waves and enhancing compression capability. But the flow angle and the efficiency decrease only 0.15° and 1 point, the reason is that the shock waves reflect many times causing the later shock waves weaken. Though there is the interaction of the shock waves and boundary layer after throat, the flow angle and the adiabatic efficiency do not decrease too much.

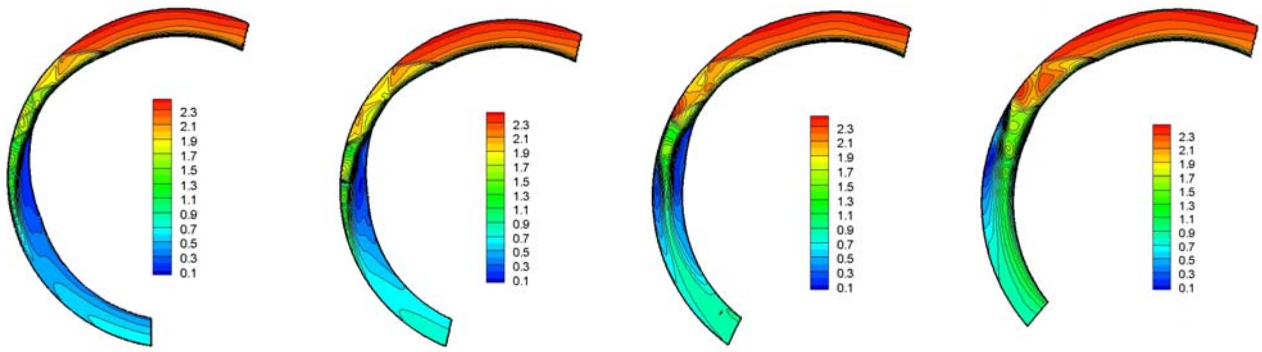

(a) case F1 (b) case F2 (c) case A1 (d) case F3

Fig. 22 Relative Mach number contour of S2 flow surface at 50% pitch of the flow-path

Table 8 Performance parameters of the ram-rotor at exit with different throat contraction ratio

Throat contraction ratio	0.6	0.7	0.8	0.9
Flow angle (°)	85.50	85.65	82.36	80.56
Adiabatic efficiency	0.7416	0.7516	0.7229	0.6838
Total pressure recovery coefficient	0.7275	0.6259	0.5731	0.5483
Total pressure ratio	12.2087	8.9070	7.0970	5.2584

According to the performance trends of the ram-rotor with different strake stagger angles (Table 5), with the increase of strake stagger angle, the total pressure ratio decreases quickly, but the adiabatic efficiency range is somewhat narrow. If the ram-rotor has a littler throat contraction ratio (such as 0.6) and a larger strake stagger angle (such as 18°), its flow angle may reduce greatly, however, its total pressure ratio will decrease more rapidly. By comprehensive consideration, case F1 has the best configuration in this paper.

Taking case F1 as an example presenting entropy and streamlines of S1 at different throat height and strake wall (Fig. 23). The starting position of the separation zone is stably located at the exit of the throat by adjusting the back pressure in computing process, so a vortex pair attaches to the hub after throat (Fig. 23(a)). Affected by strake boundary layer, this vortex pair rotates from strake wall to the middle of flow-path, weakened at 10 % throat height and almost disappeared at 20 % throat height (Fig. 23(b)-(c)). The streamlines of 50 % throat height become flat (Fig. 23(d)). The casing is ring shape without the compression surface and subsonic diffuser, so there is not any vortex (Fig. 23(g)), and the gas flow near casing is somewhat similar to the traditional compressor blades, moving from pressure surface to suction surface. This transverse flow weakened when the S1 is far from the casing (Fig. 23(e)-(f)). The right strake wall is similar to the suction surface, affected greatly by the boundary layer, and the limit streamlines converge from the hub and the casing to the middle flow-path (Fig. 23(h)); the left strake wall is similar to the pressure surface, the limit streamlines are basically parallel to the hub and the casing, and move from the casing to hub after the exit of throat (Fig. 23(i)). Near the hub, it is found that the high entropy zone occupies the whole flow-path before the exit of the throat, when the S1 is far from the hub, the high entropy zone's area contracts, weakens and moves towards the outlet (Fig. 23(a)-(c)). At the same time, the high entropy zone of casing is formed by the transverse flow (Fig. 23(g)), and the high entropy zone weakens when S1 is far from the casing (Fig. 23(e)-(f)). The high entropy zone of S1 at 50 % throat height is lowest (Fig. 23(d)).

The ram-rotor is a high speed rotating machinery and the flow field in the ram-rotor is three-dimensional. The shock loss, the interaction of the shock wave and boundary layer, and the boundary layer separation are the main factors of the flow loss. The configuration of the ram-rotor should be further optimized to decrease the shock loss, weaken the interaction of the shock wave and boundary layer, and minish the boundary layer separation's area.

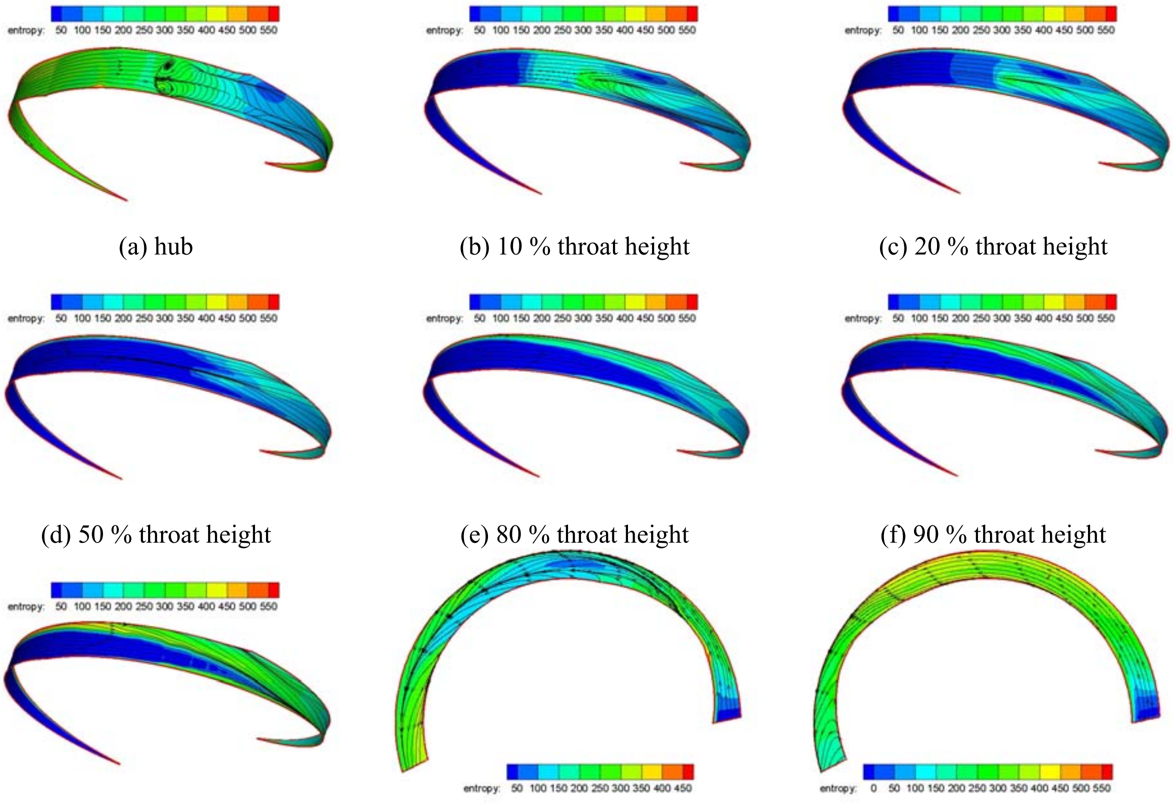

(a) hub (b) 10 % throat height (c) 20 % throat height

(d) 50 % throat height (e) 80 % throat height (f) 90 % throat height

(g) casing (h) right strake wall (i) left strake wall

Fig. 23 Entropy and streamlines of S1 at different throat height and strake wall

6 CONCLUSIONS

1. All of the six geometric parameters studied in this paper can affect the flow field structure of the ram-rotor including the number and the starting positions of the separation zones. Except the strake stagger angle and the subsonic divergent angle, the other geometric parameters can also affect the number of the shock waves and their distribution in the flow-path of the ram-rotor.

2. From the results of the numerical simulation, it is found that the strake stagger angle and the throat contraction ratio have more obvious effect on the performance of the ram-rotor than other geometric parameters. The larger strake stagger angle can bring a smaller flow angle and greater mass flow rate, and reduce the adiabatic efficiency, the total pressure recovery coefficient and the total pressure ratio. It is beneficial to choose small throat contract ratio for increasing the total pressure ratio, the total pressure recovery coefficient and the adiabatic efficiency, but the choice of the flow angle should be compromised. The comprehensive performance of case F1 is the best case among theses cases with different geometric parameters.

3. In order to gain preferable overall performance of the ram-rotor, the strake wall section with the positive trapezoid shape is better than that with the reversed trapezoid shape. The small throat length-height ratio will decrease the adiabatic efficiency and the total pressure ratio; and the big throat length-

height ratio will increase the flow angle and the width of the ram-rotor. The flow angle can be increase with small compression ramp and the total pressure ratio be decrease with large compression ramp. The small subsonic divergent angle leads to the decreasing of the adiabatic efficiency and total pressure ratio, and the large subsonic divergent angle can make the flow angle at exit increase rapidly.

4. In order to improve the overall performance and the flow field structure of the ram-rotor, the reasonable compromises should be made among the adiabatic efficiency, the total pressure ratio, the total pressure recovery coefficient, the flow angle, the mass flow rate, the width of the ram-rotor, and so on. In addition, except the six geometric parameters above, there are lots of research work needed to be carried out in-depth such as the influence of the exit-inlet area ratio and the tip clearance of the ram-rotor on the performance of the ram-rotor.

REFERENCES

[1] Ramgen Power Systems. Shock Compression- What is it? http://www.ramge-n.com/tech_shock_what is it.html, 2005

[2] Ramgen Power Systems. Shock Compression-Flight Applications of Shock Compression. http://www. ramgen.com/tech_shock_flightapps.html, 2005

[3] M. Valorani, F. Nasuti, M. Onofri, etal. Optimal Supersonic Intake Design for Air Collection Engines (ACE). Acta Astronautica, 1999, 45(12):729~745

[4] U. Ahsun, A. Merchant, J. D. Paduano, etal. Design of a Near-isentropic Supersonic Inlet Using Active Control. Journal of Propulsion and Power.2005, 21(2): 292~299

[5] Shawn P. Lawlor, John B. Hinkey, Steven G. Machin, etal, Supersonic compression stage design & test results[C]. IMEC2004-59914, 2004.

[6] Allan D. Grosvenor, Paul M. Brown, Shawn P. Lawlor. Design methodology and predicted performance for a supersonic compressor stage[C]. ASME paper GT2006-90409, 2006.

[7] Victor de Biasi. 485-kW turbine rated 35% simple cycle at 1700F firing temperature[J]. Gas Turbine World, 2002, 32(5):13-16

[8] Ramgen Power Systems. The Rampressor Competitive Advantages. http://www.ramgen.com/ tech_shock_ rampressoradv.html, 2005

[9] Robert Steel, Peter Baldwin, James Kesseli. Insertion of shock wave compression technology into micro turbines for increased efficiency and reduced costs[C]. ASME paper GT2005-68203, 2005.

[10] S. P. Lawlor, P. Baldwin. Conceptual Design of a Supersonic CO_2 Compressor. ASME Paper GT2005-68349, 2005

[11] R. Steele, P. Baldwin, J. Kesseli. Insertion of Shock Wave Compression Technology into Micro Turbine for Increased Efficiency and Reduced Costs. ASME Paper GT2005-68203, 2005

[12] A. D. Grosvenor, P. M. Brown, S. P. Lawlor. Design Methodology and Predicted Performance for a Supersonic Compressor Stage. ASME Paper GT2006-90409, 2006

[13] S. P. Lawlor, R. C. Steele, P. Baldwin. Advanced Supersonic Component Engine for Military Applications. ASME Paper GT2007-27336, 2007

[14] K. D. Broichhausen, K. U. Ziegler. Supersonic and Transonic Compressores: Past, Status and Technology Trends. ASME Paper GT2005-69067, 2005

[15] LI Yong, LIU Zhi-you, AN Yi-ran. A brief introduction to Fluent—a general purpose CFD code [J].Journal of Hydrodynamics, 2001, 16(2):254-258.

[16] YAO Zheng, CHEN Kang-min. Review on the commercial CFD softwares[J]. Journal of University of Shanghai for Science and Technology, 2002,24(2):137-144.

[17] A. Schneider, Wolfgang W. Koschel. Detailed analysis of a mixed compression hypersonic intake [C]. ISABE paper 99-7036, 1999.